

---

# Sampling 3D Gaussian Scenes in Seconds with Latent Diffusion Models

---

Paul Henderson<sup>1</sup> Melonie de Almeida<sup>1</sup> Daniela Ivanova<sup>1</sup> Titas Anciukevičius<sup>2</sup>  
<sup>1</sup> University of Glasgow <sup>2</sup> University of Edinburgh

## Abstract

We present a latent diffusion model over 3D scenes, that can be trained using only 2D image data. To achieve this, we first design an autoencoder that maps multi-view images to 3D Gaussian splats, and simultaneously builds a compressed latent representation of these splats. Then, we train a multi-view diffusion model over the latent space to learn an efficient generative model. This pipeline does not require object masks nor depths, and is suitable for complex scenes with arbitrary camera positions. We conduct careful experiments on two large-scale datasets of complex real-world scenes – MVImgNet and RealEstate10K. We show that our approach enables generating 3D scenes in as little as 0.2 seconds, either from scratch, from a single input view, or from sparse input views. It produces diverse and high-quality results while running an order of magnitude faster than non-latent diffusion models and earlier NeRF-based generative models.

## 1 Introduction

Learning generative models that capture the distribution of the 3D world around us is a compelling yet challenging problem. As well as the grander aim of building intelligent agents that can understand their environment, such models are also useful for many practical tasks. In games and visual effects, they enable effortless creation of 3D assets, which currently is notoriously difficult, slow and expensive. In computer vision, they enable 3D reconstruction of realistic scenes from a single image, with the generative model synthesising plausible 3D details even for regions not visible in the image—unlike classical 3D reconstruction methods [35, 64].

Large-scale datasets of images, text and video [83, 29, 7] have enabled learning impressive generative models for those modalities [78, 73, 41]. However, there are no extant large-scale datasets of photorealistic 3D scenes. Existing 3D datasets are either large but consist primarily of isolated objects (not full scenes), often with unrealistic textures [118, 22, 12]; or they are photorealistic environments (captured with 3D scanners) but too small for learning a generative model over [21, 4]. In contrast, large-scale in-the-wild datasets of *multi-view images* are now readily available [128, 135, 74].

It is therefore desirable to learn 3D generative models directly from datasets of multi-view images, rather than from 3D data. One naïve strategy is to apply standard 3D reconstruction techniques to every scene in such a dataset, then train a 3D generative model directly on the resulting reconstructions [65, 129]. However, this is computationally expensive. It also leads to a challenging learning task for the generative model, since by reconstructing scenes independently we do not obtain a smooth, shared space of representations (e.g. similar scenes may have very different weights when represented as a NeRF [64]). This makes it difficult to learn a prior that generalises, rather than simply memorising individual scenes. These limitations have inspired a line of works that learn 3D generative models directly from images [3, 96, 84, 38]. Unfortunately, recent methods are very slow to sample, since they require expensive volumetric rendering operations after every step of a diffusion process [96, 2, 102].

In this work, we design an efficient generative model for 3D scenes that is trained using only posed multi-view images. Our key idea is to learn an autoencoder on multi-view images, that simultaneously

builds a structured 3D representation while also compressing this into a lower dimensionality latent space. We can then train a denoiser on the resulting latent representations, and perform the expensive iterative denoising process in this much lower-dimensional space. Unlike previous 3D-aware diffusion models [96, 102], the rendering operation is *not* inside the sampling loop.

We adopt Gaussian Splats [48] as our 3D representation. Recent work on 3D reconstruction has shown splats achieve a favorable trade-off between reconstruction quality and training/rendering speed. The original work of Kerbl *et al.* [48] considered only reconstruction from densely-captured images, but several more recent works aim to predict splats from one or few images [17, 13, 97, 130, 124]. However, unlike ours, these methods are not generative – they do not capture a *distribution* over 3D scenes. They therefore cannot predict the full space of scenes consistent with the input images; nor can they perform other tasks such as unconditional or class-conditional generation. Score distillation [72, 108] provides a way to leverage 2D generative models for 3D content synthesis, but such methods neither learn nor sample a true 3D prior, and so are still prone to undesirable artifacts [99, 123, 19].

Our proposed model is very fast, since it benefits from the efficient rendering and optimisation of Gaussian Splats, and also from the speed-up provided by diffusion over a compressed latent space. This enables sampling a full batch of eight 3D scenes in just 1.6s—more than  $20\times$  faster than the fastest existing 3D-aware diffusion model [96]. In addition, our model has the following desirable features: (i) it can represent arbitrarily large scenes, by placing 3D content anywhere in the view frustum of the cameras (in particular, it is not limited to pre-segmented or object-centric scenes); (ii) it supports several tasks—unconditional generation, single-image 3D reconstruction, sparse-view 3D reconstruction, depending on the conditioning signal provide during inference; (iii) it does not rely on any depth or segmentation estimates or annotations for training—it can be trained from scratch using only posed multi-view images.

To summarise, our core contribution is **the first generative model that learns and samples a distribution over real-world scenes represented as Gaussian Splats**. Our technical contributions that enable this are: (i) we design a new 3D-aware autoencoder architecture that learns to represent multi-view images via a compressed latent space, that can be decoded to Gaussian Splats; (ii) we demonstrate how diverse and realistic 3D scenes can be sampled efficiently with a diffusion model on the latent representation, either unconditionally or conditioned on an input image; (iii) we show that for a given compute budget, our latent approach gives significantly better results for both unconditional generation and generative reconstruction.

## 2 Related Work

**Reconstruction from dense views.** Numerous scene representations and corresponding inference methods have been proposed, including surface representations (e.g. meshes, distance fields [70]), point clouds [82, 86, 93], light fields [20, 32] and volumetric representations (e.g. radiance fields [120] and voxels [87, 91]). Current state-of-the-art methods use neural radiance fields (NeRFs) [64, 5], which implicitly parameterize a radiance field with a neural network, making them easily optimizable with gradient descent by minimizing an image reconstruction loss. However, NeRFs require expensive volumetric rendering involving numerous MLP queries, and despite recent efforts to reduce their size [71, 28, 2, 66, 55, 14, 121, 28], both training and rendering remain slow. Recently, Gaussian Splatting [48] was introduced as an alternative that allows real-time rendering and fast training, with quality approaching that of state-of-the-art NeRFs. Our work also uses this efficient representation, but instead of fitting individual scenes, we build a generative model that learns to sample them from a distribution (e.g. conditioned on a class label or sparse set of images).

**Reconstruction from sparse views.** While the above methods can reconstruct 3D from dense (e.g.  $>50$ ) sets of images, in practice, parts of a scene cannot be observed from multiple images and need to be inferred. To solve this, a line of work trains models to reconstruct 3D scenes from fewer (e.g.  $<10$ ) views. Most approaches [126, 110, 15, 60, 39, 115, 60, 116, 76] unproject 2D image features into 3D space, fuse them and apply NeRF rendering. Several recent and concurrent methods [13, 17, 139, 130, 124, 133, 114, 88, 97] tackle the sparse-view reconstruction task using splats as the 3D representation; others aim to predict novel views directly, without explicit 3D [53, 79, 25]. However, these methods are not probabilistic—they do not represent uncertainty about unobserved parts of the scene (e.g. the back of an object). As a result, instead of sampling one of many plausible 3D representations, these methods output a single average solution. For example, *MVSplat* [17] and

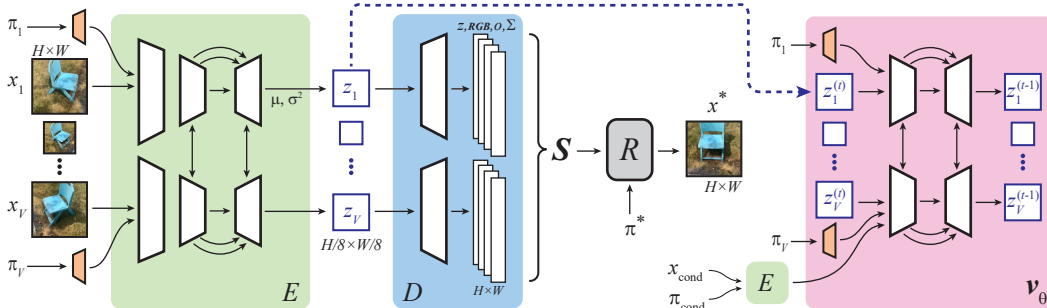


Figure 1: Overview of our latent diffusion model for 3D scene synthesis. **Left:** We train an autoencoder, that encodes (green box;  $E$ ) multi-view images  $\{x_v\}_1^V$  to a compressed latent space  $\{z_v\}_1^V$ . It simultaneously learns to decode (blue box;  $D$ ) the latents to parameters of Gaussian splats  $\mathcal{S}$ , which can then be rendered back to images  $x^*$ . **Right:** We train a denoising diffusion model (pink box;  $v_\theta$ ) over the multi-view latent features  $z_v$ . This supports unconditional generation, or generation conditioned on an input image  $x_{\text{cond}}$  (itself encoded with  $E$ ). Following the efficient, low-dimensional denoising process, the resulting latents are mapped back to a 3D scene by  $D$ .

*pixelSplat* [13] train a network to map context images to 3D splats, but lack the ability to generate 3D scenes unconditionally or to sample diverse completions for occluded regions. *latentSplat* [114] does construct a posterior distribution over splats then sample this—however it imposes a mean-field (independent) posterior on the splat parameters themselves, meaning it cannot capture complex posterior dependencies in the scene geometry, and thus cannot sample coherent shapes for unobserved areas of scenes. Note that almost all the above methods are designed for two or more input views. Only SplatImage [97] can predict 3D splats from a single image, and even this method is limited to masked, object-centric scenes. While some approaches incorporate information from generative models ad-hoc to increase plausibility of uncertain regions [89, 77, 138, 63, 19, 69], they do not learn to sample the true posterior distribution on scenes, which our method aims to learn.

**Generative models.** Diverse families of generative models [50, 31, 106, 47, 94, 42] have been proposed to learn complex distributions from training data. With the success of generative models across various modalities, including language [107, 73], sound [105], and images [78, 41], there is now a growing interest in sampling 3D content. A straightforward approach is to create a large-scale 3D dataset [12, 22] and train a generative model directly on this [62, 104, 16, 134, 45, 54, 18, 65, 6, 111, 49, 90, 34, 46, 33]. However, unlike other modalities, large-scale, highly-realistic 3D datasets of scenes are challenging to create, and most 3D representations lack shared structure (as each datapoint is created independently, e.g. meshes have different topologies, and point-clouds different numbers of points) making learning priors difficult. While recent works use autodecoding [6] or optimal transport to share structure across representations [129], these methods have been limited to small or object-centric datasets.

To circumvent the difficulty of learning a smooth prior over independently-reconstructed scenes, various methods learn a 3D-aware generative model directly from images. A simple yet elegant approach [26, 117, 7, 11, 103, 58, 101, 127, 113, 51, 100, 59, 57, 44, 30, 98] is to generate multi-view images conditioned on camera poses without an explicit 3D representation, then reconstruct 3D from the generated images using classical 3D reconstruction methods. However, it inherits the limitations of classical methods, primarily the need to generate a large number of consistent images (>50) and the absence of priors in the 3D reconstruction process.

To directly sample 3D representations, some works learn 3D-aware generative models of 2D images, which retain the mathematical formulation of generative image models, but introduce priors into the network architecture which force the model to output images via an explicit 3D representation. Seminal approaches were based on VAEs [52, 36, 38, 1, 37] and GANs [84, 10, 92, 23, 68, 67, 132, 24], while current state-of-the-art methods use 3D-aware denoising diffusion models [3, 46, 96, 102, 122, 2, 43, 85, 9]. Unlike score-distillation methods [72, 112, 99, 123, 136, 125, 119, 137, 56, 109] that suffer from mode-seeking behavior and do not truly sample a distribution, 3D-aware diffusion models can sample 3D scenes from the true posterior distribution. However, existing works use radiance fields to represent the scene and thus are limited by slow training, sampling, and rendering

times. In contrast, our work samples 3D scenes in less than a second (0.2s) compared to 5.4s for the recent [96] or 51s for [2]; ours can also render the sampled 3D asset in real-time.

### 3 Method

Our goal is to build a model supporting conditional and unconditional generation of 3D scenes. We assume access only to a training dataset of multi-view images with camera poses (readily available from phone cameras or COLMAP SfM [82]). We do not require any additional 2D/3D supervision (e.g. annotations, pretrained models, foreground masks, depth-maps) and we do not assume that camera poses are aligned consistently across the dataset.

We achieve this by designing a latent diffusion framework that is trained in two stages. First, a 3D-aware variational autoencoder (VAE) is trained on sets of multi-view images (Sec.3.1). It encodes multi-view images to a compact latent representation, decodes this to an explicit 3D scene represented by Gaussian Splats, then renders the scene to reconstruct images. Second, we train a denoising diffusion model on the compact latent space learnt by the autoencoder (Sec.3.2). This diffusion model is trained jointly for class-conditional and image-conditional generation, and can efficiently learn a distribution on the latent space. During inference, the resulting latents are decoded back to splats by the autoencoder, and rendered.

#### 3.1 Autoencoder

Our autoencoder takes as input  $V$  views  $\mathbf{x} = \{x_v\}_{v=1}^V$  of a scene (each of size  $H \times W$  pixels), with their relative camera poses  $\boldsymbol{\pi} = \{\pi_v\}_{v=1}^V$ . It processes these jointly to give a set of splats  $\mathcal{S}$ , such that rendering  $\mathcal{S}$  from each  $\pi_v$  should reconstruct the original image  $x_v$ . Importantly, it passes all information about the scene through a low-dimensional latent bottleneck, yielding a compressed representation from which the splats are then decoded and rendered.

**Encoding multi-view images.** The  $x_v$  are first passed independently through three downsampling residual blocks similar to [27, 78], yielding feature maps of resolution  $\frac{H}{8} \times \frac{W}{8}$ . These features are processed by a multi-view U-Net [80], which enables the different views to exchange information efficiently (necessary to achieve a consistent 3D reconstruction). This U-Net is based closely on [42]. To adapt it to our multi-view setting, we take inspiration from video diffusion models, notably [8], and add a small cross-view ResNet after each block that combines information from all views, for each pixel independently. We also modify all attention layers to jointly attend across features from all views. Aside from these parts, all the remainder of processing by residual blocks treats views independently. The final convolution of the U-Net outputs the mean and log-variances of a feature-map of size  $\frac{H}{8} \times \frac{W}{8}$  for each view. This will be the compressed latent space  $\{z_v\}_{v=1}^V$  in which we perform denoising (see Sec.3.2), and so we restrict it to have only very few channels. We assume a diagonal Gaussian posterior distribution, following common practice for VAEs [50, 78]. We denote the overall encoder mapping from  $\{x_v\}_{v=1}^V$  to a latent sample  $\{z_v\}_{v=1}^V$  by  $E$ ; it is shown by the green box in Fig. 1.

**Decoding to a 3D scene.** The latent features  $\{z_v\}_{v=1}^V$  are decoded to a 3D scene  $\mathcal{S}$  represented as Gaussian Splats [48]. Specifically, we pass the features through three upsampling residual blocks, mirroring the initial layers of  $E$ ; this yields feature maps with the same size as the original images. Similarly to [97, 13], the features for each view are mapped by a convolution layer to parameters of splats supported on the view frustum. For each pixel, we predict the depth, opacity, RGB color, rotation and scale of a corresponding splat; in total this requires 12 channels. The 3D position of each splat is then calculated by unprojecting it along the corresponding camera ray by the predicted depth. The union of the  $V \times H \times W$  splats across all images constitutes our scene representation  $\mathcal{S}$ . This representation (aptly termed a *splatter image* in [97]) provides a structured way to represent splats, allowing reasoning over them with standard convolutional layers instead of permutation-invariant layers necessary for unstructured point-clouds. We denote the mapping from  $\{z_v\}_{v=1}^V$  to  $\mathcal{S}$  by  $D$ ; it is shown by the blue box in Fig. 1. The splats  $\mathcal{S}$  can then be rendered to pixels  $x^*$  using arbitrary camera parameters  $\pi^*$ ; we denote this rendering operation by  $x^* = R(\mathcal{S}, \pi^*)$

A key benefit of having splats supported on images at all denoised viewpoints is that we can represent 3D content anywhere we look. This contrasts with e.g. SplatterImage [97]—when performing single-



image reconstruction, they can only parameterise splats inside (or very close to) the view frustum of the input image, whereas ours can generate coherent content arbitrarily far away.

**Conditioning on pose.** In order to condition the autoencoder on the relative poses of the views, we design a novel strategy based on the splat renderer itself. For each view, we generate a set of splats along the edges of its view frustum; for each view, we assign a random color. We then render the resulting splat cloud from all cameras. These renderings are concatenated with the input  $x_v$  before the first residual block of the encoder. Note that without this conditioning, it is impossible for the autoencoder to learn the arbitrary scene scale (even if it successfully learns to triangulate the input images), due to the perspective depth/scale ambiguity.

**Training.** We assume access to minibatches containing  $V$  input views  $(\mathbf{x}^{(\text{in})}, \boldsymbol{\pi}^{(\text{in})})$ , and an additional  $V'$  nearby target views  $(\mathbf{x}^{(\text{target})}, \boldsymbol{\pi}^{(\text{target})})$  that are not passed to  $E$ . We predict splats  $S = D(E(\mathbf{x}^{(\text{in})}, \boldsymbol{\pi}^{(\text{in})}))$ , then render these at the target views giving  $x_{v'}^* = R(S, \boldsymbol{\pi}_{v'}^{(\text{target})}) \forall v' = \{1 \dots V'\}$ . The network is then trained as a variational autoencoder [50, 75], using the sum of  $L^2$  and LPIPS [131] distances between input and rendered images as a reconstruction loss, and maximising the log-probability of the sampled latents  $\{z_v\}_{v=1}^V$  under a standard Gaussian prior. This leads to the following loss:

$$\mathcal{L}_{\text{AE}} = \sum_{v'=1}^{V'} \left\{ \|x_{v'}^* - x_{v'}^{(\text{target})}\|_2^2 + \text{LPIPS}(x_{v'}^*, x_{v'}^{(\text{target})}) + \|z_v\|_2^2 \right\} \quad (1)$$

where  $\beta$  adjusts the weight of the KL loss. Note that unlike methods using NeRFs, the speed of the splat rendering operation  $R$  means we can straightforwardly apply LPIPS to full-image renderings.

**Compression.** Compared with treating the splats themselves as the latent space, our approach yields a compression factor of  $128\times$  when we use 6 latent channels (as in our main experiments). As shown in Sec. 4, this enables much more efficient training and inference for the denoiser.

### 3.2 Denoiser

We now define a denoising diffusion model over the low-dimensional multi-view latent feature maps  $\{z_v\}_{v=1}^V = \mathbf{z}$  produced by the encoder  $E$ . We take a similar approach to latent diffusion models for images [78], but instead of a 2D U-Net, use a very similar multi-view U-Net architecture as in the autoencoder (Sec. 3.1), now conditioned on the diffusion timestep, as in [42]. We condition this multi-view U-Net  $\hat{v}_\theta$  on the camera poses  $\pi_v$  in the same way as for the autoencoder, i.e. concatenating a representation of all view frusta. The U-Net is then responsible for learning the joint distribution of latent features across all views, passing information via cross-view attention and convolution operations.

**Conditional generation.** We train the denoiser jointly for image-conditional and class-conditional generation (choosing randomly which to use for each minibatch), and also dropping the conditioning entirely for 20% of minibatches to enable classifier-free guidance [40]. For class conditioning, we follow common practice and use a learnt embedding for class indices, which is added to the timestep embedding in the U-Net. For image conditioning (i.e. when performing 3D reconstruction), we again make use of our pretrained encoder  $E$ , to encode the conditioning images  $x_{\text{cond}}$  and their poses  $\pi_{\text{cond}}$ . The conditioning latents output by  $E(x_{\text{cond}}, \pi_{\text{cond}})$  are then concatenated with the noisy latents at the start of the denoiser.

**Training.** During training we sample minibatches of posed views  $(\mathbf{x}, \boldsymbol{\pi})$ . These are converted to latents  $\mathbf{z}$  by passing them to  $E$  and sampling the posterior. We normalise  $\mathbf{z}$  to have approximately zero mean and unit standard deviation, based on statistics of the first training minibatch. We then sample a diffusion timestep  $t$  and sample noisy latent from the Gaussian forward process  $\mathcal{N}(\mathbf{z}^{(t)}; \alpha_t \mathbf{z}, \sigma_t^2 \mathbf{I})$ , where  $\alpha_t$  and  $\sigma_t$  are specified by a linear noise schedule; we optimize the denoiser’s parameters  $\theta$  by gradient descent on the following loss:

$$\mathcal{L}_{\text{DDM}} = \mathbb{E}_{t, \epsilon \sim \mathcal{N}(\mathbf{0}, \mathbf{I}), \mathbf{z}^{(t)}} \|\hat{v}_\theta(\mathbf{z}^{(t)}, t) - \mathbf{v}^{(t)}\|_2^2 \quad (2)$$

Importantly, due to our abstract latent space, our implementation trains the denoiser  $\hat{v}_\theta(\mathbf{z}^{(t)}, t)$  to predict  $\mathbf{v}^{(t)} \equiv \alpha_t \epsilon - \sigma_t \mathbf{z}$  [81] which is more numerically stable than  $\mathbf{x}^{(0)}$  prediction used by other 3D-aware diffusion models [96, 2, 3] that constrain the denoiser itself to output rendered pixels.

Table 1: Results from our method and baselines on unconditional/class-conditional scene generation, 3D reconstruction from a single image, and 3D reconstruction from sparse (six) views.

|                           | Generation  |             | 1-view reconstruction |              |             | 6-view reconstruction |              |
|---------------------------|-------------|-------------|-----------------------|--------------|-------------|-----------------------|--------------|
|                           | FID ↓       | Time /s ↓   | PSNR ↑                | LPIPS ↓      | Time /s ↓   | PSNR ↑                | LPIPS ↓      |
| <b>MVImgNet</b>           |             |             |                       |              |             |                       |              |
| Ours                      | <b>23.1</b> | <b>0.22</b> | <b>20.6</b>           | <b>0.324</b> | 0.22        | <b>24.7</b>           | <b>0.184</b> |
| SplatterImage [97]        | –           | –           | 18.2                  | 0.367        | <b>0.03</b> | –                     | –            |
| <b>RealEstate10K</b>      |             |             |                       |              |             |                       |              |
| Ours                      | <b>29.5</b> | <b>0.22</b> | <b>16.4</b>           | 0.455        | 0.22        | <b>23.3</b>           | <b>0.155</b> |
| SplatterImage [97]        | –           | –           | 16.2                  | <b>0.347</b> | <b>0.03</b> | –                     | –            |
| <b>MVImgNet furniture</b> |             |             |                       |              |             |                       |              |
| Ours                      | <b>89.0</b> | <b>0.22</b> | 17.9                  | <b>0.407</b> | 0.22        | 22.9                  | 0.214        |
| GIBR [2]                  | 99.8        | 44.9        | <b>18.5</b>           | 0.414        | 44.3        | <b>25.4</b>           | <b>0.199</b> |
| Viewset Diffusion [96]    | 191.4       | 4.98        | 17.6                  | 0.540        | 4.25        | –                     | –            |
| RenderDiffusion [3, 2]    | 234.1       | 10.2        | 17.4                  | 0.622        | 10.2        | 18.4                  | 0.601        |
| PixelNeRF [126, 2]        | –           | –           | 16.6                  | 0.582        | <b>0.12</b> | 15.7                  | 0.647        |

**Sampling.** To sample a 3D scene from our model, we begin by sampling Gaussian noise  $z^{(1000)} \sim \mathcal{N}(\mathbf{0}, \mathbf{I})$  in the latent space, and choosing a set of camera poses (e.g. from a held-out validation set) as conditioning. We then use DDIM sampling [95] to find  $z^{(0)}$ , with classifier-free guidance for class conditioning. From this we decode the generated 3D scene by  $\mathcal{S} = D(z^{(0)})$ , which can then be rendered efficiently from arbitrary viewpoints  $\pi^*$  using  $R$ .

## 4 Experiments

We evaluate our model and several baselines on both generation and one-/few-view 3D reconstruction. Further implementation details for our method and the baselines are given in the appendix.

**Datasets.** We evaluate our approach on two large-scale datasets of real-world images—MVImgNet [128] and RealEstate10K [135]. MVImgNet consists of videos showing diverse objects in the wild. We use the splits from MVPNet subset, containing 87,820 videos covering 180 object classes, and restrict to 5000 scenes for evaluation. Each video typically contains 30 frames. RealEstate10K contains 69893 videos showing indoor and outdoor views of houses. We use the official splits, again limiting to 5000 scenes for evaluation. Each video typically contains 50-200 frames. We use the complete video clips (often with substantial camera motion) for training and evaluation, not the shorter, easier segments from [115]. Note that the videos in both datasets depict complete scenes, not just isolated objects. For both datasets, we center crop the images with size equal to small edge, then rescale to  $96 \times 96$ . During training, we randomly sample sets of six frames as multi-view images. We use the camera poses provided with each dataset, but only provide *relative* poses to the model. We do not require any canonicalisation of scene orientation or scale, unlike earlier methods [96, 3, 97], and do not rely on segmentation masks nor depths.

**Baselines.** We compare our approach to several existing works. **GIBR** [2] and **ViewSet Diffusion** [96] are 3D-aware diffusion models over multi-view images. They encode sets of noisy views, and uses these to build a radiance field representation of the scene that is then rendered to give the denoised images. Like our method, they support both unconditional generation and reconstruction. However, both are relatively expensive since they must perform volumetric rendering during every denoising step. **RenderDiffusion** [3] is a similar method that only requires single images during training; we use the variant adapted for the in-the-wild data by [2]. **SplatterImage** [97] is a recent deterministic method for 3D reconstruction from a single image, outputting splats from a single U-Net pass. This is currently the only method able to directly predict 3D splats from a single image. However, the original work only considers masked views of isolated objects; we therefore adapt their method to work for our larger, unmasked scenes. Lastly, **PixelNeRF** [126] predicts a radiance field deterministically by unprojecting features from one or more input images; we use the in-the-wild variant from [2].

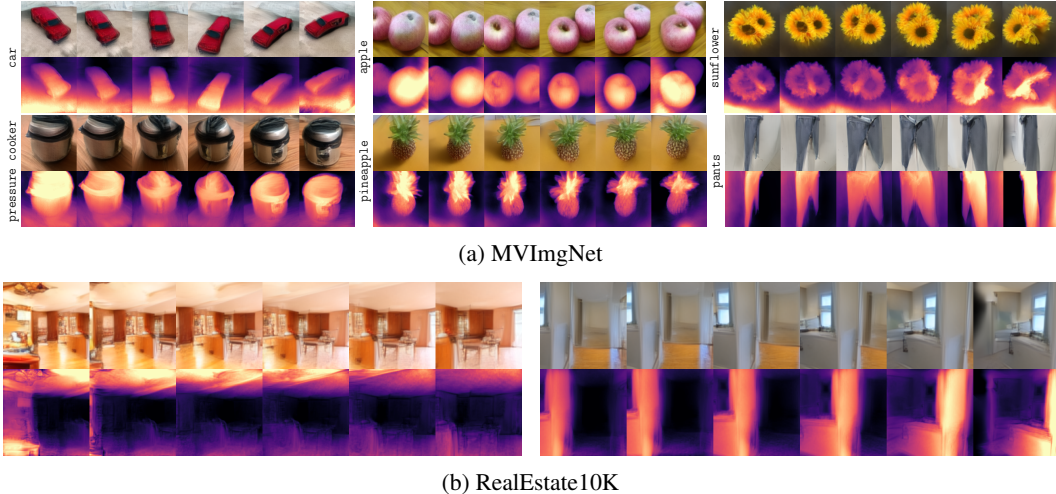


Figure 2: Qualitative examples of class-conditional (MVImgNet) and unconditional 3D generations (RealEstate10K) from our method. For each example, the top row shows six rendered views of the sampled 3D scene, while the bottom row shows the corresponding depths. Note that our model samples 3D scenes containing objects with complex shape on a realistic background.

**Generation results.** We first evaluate on unconditional generation of 3D scenes (for RealEstate10K), and class-conditional generation for the full (180 classes) MVImgNet dataset. Qualitative examples are given in Fig. 2, with more examples in the appendix. We see that our model can generate objects of diverse classes, given just the label as conditioning. The generated scenes are coherent across views, including during long camera motions in RealEstate10K. We also perform a quantitative evaluation against several existing methods. Here we closely follow the setting of [2], using the *chair*, *table* and *sofa* classes of MVImgNet. Specifically, we compare against GIBR [2], ViewSet Diffusion [96] and also the earlier RenderDiffusion [3]. The results are presented in Table 1 (bottom five rows). On class-conditional generation, our method significantly out-performs the baselines, achieving an FID of 89.0, vs 99.8 for the second best (GIBR). Moreover, it achieves this while being  $174\times$  faster than GIBR (just 0.22s for ours, vs 45s for GIBR), since it avoids the need to render an image at every denoising step, and also operates over a lower-dimensionality space.

**Single-view 3D reconstruction results.** We now evaluate generative 3D reconstruction from a single image. Given an image, we predict 11 other evenly-spaced viewpoints, and measure the accuracy of the predicted views using PSNR and LPIPS [131]. Since our method is generative (and can generate many plausible samples for a given input), we follow standard practice for stochastic prediction and draw multiple (20) samples for each scene then record the best. Here we compare against SplatterImage [97] on MVImgNet and RealEstate10K, and all other baselines on the furniture subset of MVImgNet. Qualitative results are given in Fig. 3. We see that our method can reconstruct plausible shapes from a single image, for diverse object classes and even entire rooms. Details in the input image are preserved, while plausible content is generated in occluded parts. Moreover, in Fig. 4, we show that given one image of an object, our model can sample diverse (yet plausible) texture and shape for the unobserved back of the object. Quantitative results are presented in Table 1 (‘1-view reconstruction’ columns). We see that our method performs significantly better than SplatterImage according to both PSNR and LPIPS on the full MVImgNet dataset, as well as PSNR on RealEstate10K, though SplatterImage slightly exceeds it according to LPIPS. On the MVImgNet furniture subset (following the protocol of [2], our method is best with respect to the perceptual LPIPS metric, while GIBR performs slightly better according to PSNR (which generally favors blurrier results). The older, deterministic PixelNeRF method performs worst according to both reconstruction metrics. In the appendix, we include additional quantitative results showing that our method’s quality and accuracy are comparable for images rendered from the same viewpoints as supporting the splats and latents, and images rendered from other held-out viewpoints.

We also measure the time to reconstruct a scene using each of these methods (fixing each to 50 denoising steps for fairness), processing a minibatch of 8 scenes then calculating the average time per

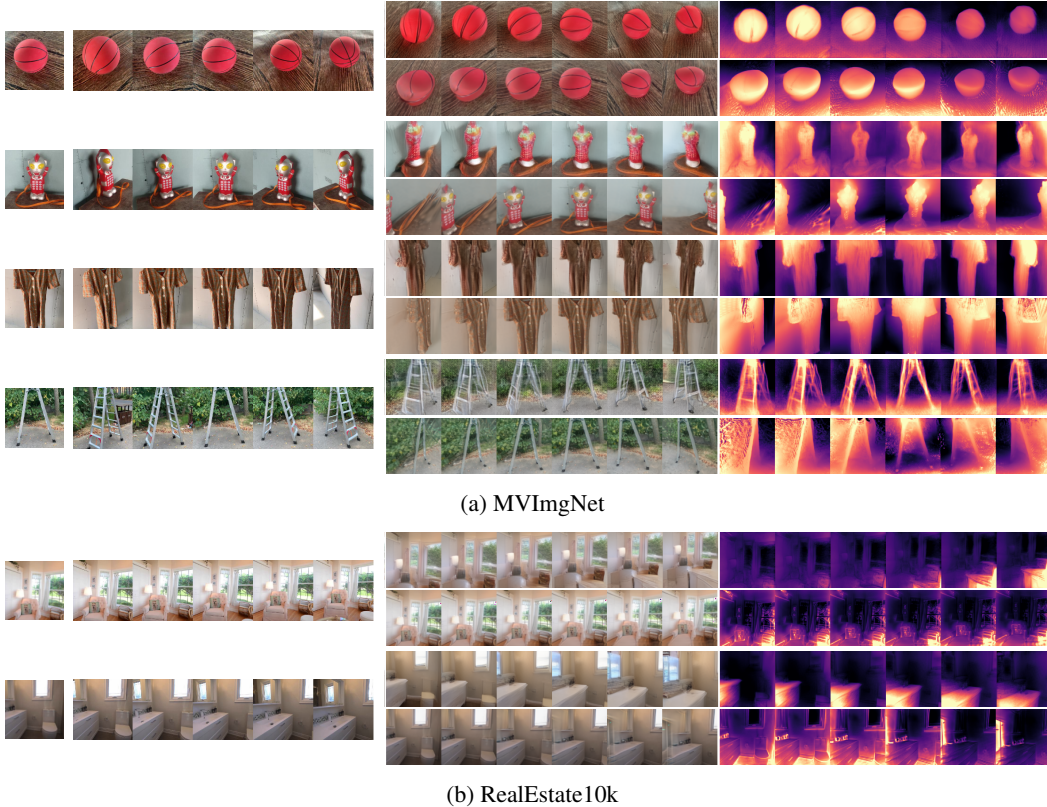


Figure 3: Qualitative comparison of 3D reconstruction from a single image between our model (top row of each scene) and SplatterImage [97] (bottom row of each scene) on MVImgNet (a) and RealEstate10k (b). The first column shows the input (conditioning) image, the second displays the ground truth images, while the third and fourth columns display the predicted frames and depths, respectively. Compared to the baseline, our model yields more plausible reconstruction, especially of the occluded regions and the background. Additional examples in the Appendix.

scene, on a single consumer GPU (NVIDIA RTX 3090). Of the generative methods, ours is by far the fastest (0.22s), compared with 4.3s for the next quickest (ViewSet Diffusion). GIBR is the slowest, taking 44s to reconstruct a scene; it is limited by the need to construct and re-render a NeRF during each denoising step. PixelNeRF is fastest overall, but trades off quality for speed and is unable to represent a posterior over 3D scenes.

**Sparse-view 3D reconstruction results.** Lastly, we evaluate reconstruction from sparse (6) views, measuring PSNR and LPIPS at six held-out views spaced equally between the inputs. Quantitative results are given in Table 1 (‘6-view reconstruction’ columns), while qualitative examples are presented in the appendix (Fig. 9). We see that qualitative reconstruction performance is very good, with fine details preserved, and plausible depth-maps. Quantitatively, our method slightly underperforms GIBR on the furniture subset of MVImgNet, although it executes much faster. Note that for this task we use only the autoencoder of our model, not the denoiser. Thus, these results also demonstrate that the autoencoder faithfully preserves details in 3D scenes, even while compressing them by  $128\times$ , justifying its use as a latent space over which to learn a generative prior.

**Benefit of being generative and latent.** We now evaluate several variants of our model, demonstrating the benefit of operating on latent space, and of treating 3D reconstruction as a generative (probabilistic) task, rather than deterministic. Results on MVImgNet are presented in Table 2. Here **Deterministic** denotes a variant of our model where the denoiser is replaced by a deterministic predictor of the latent variables representing the scene, given one input image. This model has the same network architecture as the main model, but does not sample a posterior distribution over possible scenes; instead it is expected to learn the conditional expectation in latent space. We see this scores substantially lower than our model on LPIPS, and slightly lower on PSNR. This is expected





Figure 4: Given a single input image from MVIImgNet (first column), our model performs 3D reconstruction in a generative manner, and can therefore produce multiple diverse back-views (columns 2 through 7). When compared with the back-view generated by a deterministic model (column 8), our model’s predictions are much sharper. Additional examples in the Appendix.



Figure 5: Given a single input image from RealEstate10K (first column), our model generates diverse possible completions of parts of the house that are not initially visible. In the top row, the camera moves into the doorway to the left; in the bottom row, the camera moves along the hallway. In both cases, our model generates diverse samples for the room that is revealed

since PSNR (which is based on mean square error) penalises overly-smoothed solutions less heavily than LPIPS (which prefers perceptually-correct outputs, e.g. sharp edges even if these are slightly misaligned). Moreover, qualitative results in Fig. 4 show that where our method generates many sharp, plausible samples for unobserved parts of the scene, the deterministic variant yields a blurry prediction that averages away the uncertainty. Moreover, for RealEstate10K (Fig. 5), our model can generate diverse yet plausible contents for rooms that are not visible in the input frame, e.g. when the camera moves through a doorway. **Splats-as-latents** denotes a natural ablation where instead of learning a compressed latent space, we instead treat the multi-view splat parameters themselves as the latent variables, and learn a denoiser directly over these. We train this ablation for the same duration as our main model, to fairly measure the trade-off of performance vs accuracy. We see that both generation and reconstruction performance is significantly worse than ours (57.3 vs 23.1 FID, and 0.39 vs 0.32 LPIPS). Moreover, due to the  $128\times$  larger dimensionality, this model takes more than  $60\times$  longer than ours to sample a 3D scene. Thus, for a fixed training compute budget, our latent approach yields a clear benefit in terms of quality and accuracy. Lastly, **Non-latent** is an ablation that uses a single-stage training process, similar to [2, 96]. Here the denoiser operates directly over pixels, but incorporates our splat-based scene representation within the decoder, with clean pixels given by rendering this at each denoising step. This model performs worse still (for equal training compute budget), reaching an FID of 133.8 and LPIPS of 0.499.

## 5 Conclusion

**Limitations.** While using view-supported splats enables fast optimisation and real-time rendering, our model must learn to align splats supported on different views. This sometimes leads to artifacts

Table 2: Non-generative and non-latent ablations of our method, on MVIImgNet. Note we train all models with an equal compute budget.

|                   | FID ↓       | PSNR ↑      | LPIPS ↓      | Time /s ↓   |
|-------------------|-------------|-------------|--------------|-------------|
| Full model        | <b>23.1</b> | <b>20.6</b> | <b>0.324</b> | 0.22        |
| Deterministic     | –           | 20.0        | 0.466        | <b>0.02</b> |
| Splats-as-latents | 57.3        | 19.2        | 0.389        | 13.9        |
| Non-latent        | 133.8       | 18.9        | 0.499        | 4.88        |

at the edges of objects, where splats associated with different views are slightly misaligned. Future work could explore using a hybrid 2D-3D architecture to reason over splats directly in 3D space. Also, though our model trains on in-the-wild datasets of multi-view images, we still assume that each scene is static, which prevents training on arbitrary videos. Lastly, we still require camera poses for each image; while this is easily satisfied, it would be preferable to remove this requirement.

**Conclusion.** We introduced a latent diffusion model that samples and reconstructs large real-world scenes represented as 3D Gaussians in as little as 0.2 seconds. Our evaluations showed that this model performs  $20\times$  faster than the most recent 3D-aware diffusion models whilst maintaining scene realism and enabling real-time rendering. Trained solely on posed multi-view images, without explicit supervision, our model enables the use of diverse, in-the-wild datasets and paves the way for broad adoption of generative models in the 3D domain.

## Acknowledgments and Disclosure of Funding

PH was supported in part by the Royal Society (RGS\R2\222045). DI was supported by EPSRC (EP/R513222/1). TA was supported in part by an EPSRC Doctoral Training Partnership.

## References

- [1] T. Anciukevičius, P. Fox-Roberts, E. Rosten, and P. Henderson. Unsupervised causal generative understanding of images. *Advances in Neural Information Processing Systems*, 35:37037–37054, 2022.
- [2] T. Anciukevičius, F. Manhardt, F. Tombari, and P. Henderson. Denoising diffusion via image-based rendering. In *The Twelfth International Conference on Learning Representations*, 2024.
- [3] T. Anciukevičius, Z. Xu, M. Fisher, P. Henderson, H. Bilen, N. J. Mitra, and P. Guerrero. Renderdiffusion: Image diffusion for 3d reconstruction, inpainting and generation. In *Proceedings of the IEEE/CVF Conference on Computer Vision and Pattern Recognition (CVPR)*, pages 12608–12618, June 2023.
- [4] I. Armeni, S. Sax, A. R. Zamir, and S. Savarese. Joint 2d-3d-semantic data for indoor scene understanding. *arXiv preprint arXiv:1702.01105*, 2017.
- [5] J. T. Barron, B. Mildenhall, M. Tancik, P. Hedman, R. Martin-Brualla, and P. P. Srinivasan. Mip-nerf: A multiscale representation for anti-aliasing neural radiance fields. In *Proceedings of the IEEE/CVF International Conference on Computer Vision*, pages 5855–5864, 2021.
- [6] M. A. Bautista, P. Guo, S. Abnar, W. Talbott, A. Toshev, Z. Chen, L. Dinh, S. Zhai, H. Goh, D. Ulbricht, A. Dehghan, and J. Susskind. Gaudi: A neural architect for immersive 3d scene generation. In *NeurIPS*, 2022.
- [7] A. Blattmann, T. Dockhorn, S. Kulal, D. Mendelevitch, M. Kilian, D. Lorenz, Y. Levi, Z. English, V. Voleti, A. Letts, et al. Stable video diffusion: Scaling latent video diffusion models to large datasets. *arXiv preprint arXiv:2311.15127*, 2023.
- [8] A. Blattmann, R. Rombach, H. Ling, T. Dockhorn, S. W. Kim, S. Fidler, and K. Kreis. Align your latents: High-resolution video synthesis with latent diffusion models. In *IEEE Conference on Computer Vision and Pattern Recognition (CVPR)*, 2023.
- [9] A. Cao, J. Johnson, A. Vedaldi, and D. Novotny. Lightplane: Highly-scalable components for neural 3d fields. *ArXiv*, 2024.
- [10] E. R. Chan, C. Z. Lin, M. A. Chan, K. Nagano, B. Pan, S. D. Mello, O. Gallo, L. Guibas, J. Tremblay, S. Khamis, T. Karras, and G. Wetzstein. Efficient geometry-aware 3D generative adversarial networks. In *CVPR*, 2022.
- [11] E. R. Chan, K. Nagano, J. J. Park, M. Chan, A. W. Bergman, A. Levy, M. Aittala, S. D. Mello, T. Karras, and G. Wetzstein. Generative novel view synthesis with 3d-aware diffusion models. In *IEEE International Conference on Computer Vision (ICCV)*, October 2023.
- [12] A. X. Chang, T. Funkhouser, L. Guibas, P. Hanrahan, Q. Huang, Z. Li, S. Savarese, M. Savva, S. Song, H. Su, et al. Shapenet: An information-rich 3d model repository. *arXiv preprint arXiv:1512.03012*, 2015.
- [13] D. Charatan, S. Li, A. Tagliasacchi, and V. Sitzmann. pixelsplat: 3d gaussian splats from image pairs for scalable generalizable 3d reconstruction. *arXiv preprint arXiv:2312.12337*, 2023.
- [14] A. Chen, Z. Xu, A. Geiger, J. Yu, and H. Su. Tensorf: Tensorial radiance fields. In *Computer Vision – ECCV 2022: 17th European Conference, Tel Aviv, Israel, October 23–27, 2022, Proceedings, Part XXXII*, page 333–350, Berlin, Heidelberg, 2022. Springer-Verlag.

- [15] A. Chen, Z. Xu, F. Zhao, X. Zhang, F. Xiang, J. Yu, and H. Su. Mvsnerf: Fast generalizable radiance field reconstruction from multi-view stereo. In *Proceedings of the IEEE/CVF International Conference on Computer Vision*, pages 14124–14133, 2021.
- [16] H. Chen, J. Gu, A. Chen, W. Tian, Z. Tu, L. Liu, and H. Su. Single-stage diffusion nerf: A unified approach to 3d generation and reconstruction. In *ICCV*, 2023.
- [17] Y. Chen, H. Xu, C. Zheng, B. Zhuang, M. Pollefeys, A. Geiger, T.-J. Cham, and J. Cai. Mvsplat: Efficient 3d gaussian splatting from sparse multi-view images. *arXiv preprint arXiv:2403.14627*, 2024.
- [18] Y.-C. Cheng, H.-Y. Lee, S. Tuyakov, A. Schwing, and L. Gui. SDFusion: Multimodal 3d shape completion, reconstruction, and generation. In *CVPR*, 2023.
- [19] J. Chung, S. Lee, H. Nam, J. Lee, and K. M. Lee. Luciddreamer: Domain-free generation of 3d gaussian splatting scenes. *arXiv preprint arXiv:2311.13384*, 2023.
- [20] B. Curless and M. Levoy. A volumetric method for building complex models from range images. In *Proceedings of the 23rd annual conference on Computer graphics and interactive techniques*, pages 303–312, 1996.
- [21] A. Dai, A. X. Chang, M. Savva, M. Halber, T. Funkhouser, and M. Nießner. Scannet: Richly-annotated 3d reconstructions of indoor scenes. In *Proc. Computer Vision and Pattern Recognition (CVPR), IEEE*, 2017.
- [22] M. Deitke, R. Liu, M. Wallingford, H. Ngo, O. Michel, A. Kusupati, A. Fan, C. Laforte, V. Voleti, S. Y. Gadre, et al. Objaverse-xl: A universe of 10m+ 3d objects. *Advances in Neural Information Processing Systems*, 36, 2024.
- [23] Y. Deng, J. Yang, J. Xiang, and X. Tong. Gram: Generative radiance manifolds for 3d-aware image generation. In *IEEE Computer Vision and Pattern Recognition*, 2022.
- [24] T. Devries, M. Á. Bautista, N. Srivastava, G. W. Taylor, and J. M. Susskind. Unconstrained scene generation with locally conditioned radiance fields. *2021 IEEE/CVF International Conference on Computer Vision (ICCV)*, pages 14284–14293, 2021.
- [25] Y. Du, C. Smith, A. Tewari, and V. Sitzmann. Learning to render novel views from wide-baseline stereo pairs. In *Proceedings of the IEEE/CVF Conference on Computer Vision and Pattern Recognition*, 2023.
- [26] S. A. Eslami, D. J. Rezende, F. Besse, F. Viola, A. S. Morcos, M. Garnelo, A. Ruderman, A. A. Rusu, I. Danihelka, K. Gregor, et al. Neural scene representation and rendering. *Science*, 360(6394):1204–1210, 2018.
- [27] P. Esser, R. Rombach, and B. Ommer. Taming transformers for high-resolution image synthesis. In *Proceedings of the IEEE/CVF conference on computer vision and pattern recognition*, pages 12873–12883, 2021.
- [28] S. Fridovich-Keil, G. Meanti, F. R. Warburg, B. Recht, and A. Kanazawa. K-planes: Explicit radiance fields in space, time, and appearance. In *Proceedings of the IEEE/CVF Conference on Computer Vision and Pattern Recognition*, pages 12479–12488, 2023.
- [29] L. Gao, S. Biderman, S. Black, L. Golding, T. Hoppe, C. Foster, J. Phang, H. He, A. Thite, N. Nabeshima, S. Presser, and C. Leahy. The Pile: An 800gb dataset of diverse text for language modeling. *arXiv preprint arXiv:2101.00027*, 2020.
- [30] R. Gao, A. Holynski, P. Henzler, A. Brussee, R. Martin-Brualla, P. Srinivasan, J. T. Barron, and B. Poole. Cat3d: Create anything in 3d with multi-view diffusion models. *arXiv:2405.10314*, 2024.
- [31] I. Goodfellow, J. Pouget-Abadie, M. Mirza, B. Xu, D. Warde-Farley, S. Ozair, A. Courville, and Y. Bengio. Generative adversarial nets. *Advances in neural information processing systems*, 27, 2014.
- [32] S. J. Gortler, R. Grzeszczuk, R. Szeliski, and M. F. Cohen. The lumigraph. In *Proceedings of the 23rd annual conference on Computer graphics and interactive techniques*, pages 43–54, 1996.
- [33] J. Gu, Q. Gao, S. Zhai, B. Chen, L. Liu, and J. Susskind. Learning controllable 3d diffusion models from single-view images. *ArXiv*, 2023.
- [34] A. Gupta, W. Xiong, Y. Nie, I. Jones, and B. Oğuz. 3dgen: Triplane latent diffusion for textured mesh generation. *arXiv preprint arXiv:2303.05371*, 2023.
- [35] R. Hartley and A. Zisserman. *Multiple view geometry in computer vision*. Cambridge university press, 2003.
- [36] P. Henderson and V. Ferrari. Learning single-image 3D reconstruction by generative modelling of shape, pose and shading. *International Journal of Computer Vision (IJCV)*, 2019.
- [37] P. Henderson, C. H. Lampert, and B. Bickel. Unsupervised video prediction from a single frame by estimating 3d dynamic scene structure. *CoRR*, abs/2106.09051, 2021.

- [38] P. Henderson, V. Tsiminaki, and C. Lampert. Leveraging 2D data to learn textured 3D mesh generation. In *IEEE Conference on Computer Vision and Pattern Recognition (CVPR)*, 2020.
- [39] P. Henzler, J. Reizenstein, P. Labatut, R. Shapovalov, T. Ritschel, A. Vedaldi, and D. Novotny. Unsupervised learning of 3d object categories from videos in the wild. In *Proceedings of the IEEE/CVF Conference on Computer Vision and Pattern Recognition*, pages 4700–4709, 2021.
- [40] J. Ho. Classifier-free diffusion guidance. *ArXiv*, abs/2207.12598, 2022.
- [41] J. Ho, W. Chan, C. Saharia, J. Whang, R. Gao, A. Gritsenko, D. P. Kingma, B. Poole, M. Norouzi, D. J. Fleet, et al. Imagen video: High definition video generation with diffusion models. *arXiv preprint arXiv:2210.02303*, 2022.
- [42] J. Ho, A. Jain, and P. Abbeel. Denoising diffusion probabilistic models. *Advances in Neural Information Processing Systems*, 33:6840–6851, 2020.
- [43] L. Höllein, A. Božič, N. Müller, D. Novotny, H.-Y. Tseng, C. Richardt, M. Zollhöfer, and M. Nießner. Viewdiff: 3d-consistent image generation with text-to-image models. In *Proceedings of the IEEE/CVF Conference on Computer Vision and Pattern Recognition*, 2024.
- [44] H. Hu, Z. Zhou, V. Jampani, and S. Tulsiani. Mvd-fusion: Single-view 3d via depth-consistent multi-view generation. In *CVPR*, 2024.
- [45] K.-H. Hui, R. Li, J. Hu, and C.-W. Fu. Neural wavelet-domain diffusion for 3d shape generation. In *SIGGRAPH Asia 2022 Conference Papers*, pages 1–9, 2022.
- [46] A. Karnewar, A. Vedaldi, D. Novotny, and N. Mitra. Holodiffusion: Training a 3d diffusion model using 2d images. *ArXiv*, 2023.
- [47] T. Karras, S. Laine, and T. Aila. A style-based generator architecture for generative adversarial networks. In *Proceedings of the IEEE/CVF Conference on Computer Vision and Pattern Recognition*, pages 4401–4410, 2019.
- [48] B. Kerbl, G. Kopanas, T. Leimkühler, and G. Drettakis. 3d gaussian splatting for real-time radiance field rendering. *ACM Transactions on Graphics*, 42(4):1–14, 2023.
- [49] S. W. Kim, B. Brown, K. Yin, K. Kreis, K. Schwarz, D. Li, R. Rombach, A. Torralba, and S. Fidler. Neuralfield-ldm: Scene generation with hierarchical latent diffusion models. In *IEEE Conference on Computer Vision and Pattern Recognition (CVPR)*, 2023.
- [50] D. P. Kingma and M. Welling. Auto-encoding variational bayes. In Y. Bengio and Y. LeCun, editors, *2nd International Conference on Learning Representations, ICLR 2014, Banff, AB, Canada, April 14-16, 2014, Conference Track Proceedings*, 2014.
- [51] X. Kong, S. Liu, X. Lyu, M. Taher, X. Qi, and A. J. Davison. Eschnet: A generative model for scalable view synthesis. *arXiv preprint arXiv:2402.03908*, 2024.
- [52] A. R. Kosiorok, H. Strathmann, D. Zoran, P. Moreno, R. Schneider, S. Mokrá, and D. J. Rezende. Nerf-vae: A geometry aware 3d scene generative model. In M. Meila and T. Zhang, editors, *Proceedings of the 38th International Conference on Machine Learning, ICML 2021, 18-24 July 2021, Virtual Event*, volume 139 of *Proceedings of Machine Learning Research*, pages 5742–5752. PMLR, 2021.
- [53] J. Kulhánek, E. Derner, T. Sattler, and R. Babuška. Viewformer: Nerf-free neural rendering from few images using transformers. In *European Conference on Computer Vision (ECCV)*, 2022.
- [54] M. Li, Y. Duan, J. Zhou, and J. Lu. Diffusion-sdf: Text-to-shape via voxelized diffusion. In *Proceedings of the IEEE Conference on Computer Vision and Pattern Recognition (CVPR)*, 2023.
- [55] Z. Li, T. Müller, A. Evans, R. H. Taylor, M. Unberath, M.-Y. Liu, and C.-H. Lin. Neuralangelo: High-fidelity neural surface reconstruction. In *IEEE Conference on Computer Vision and Pattern Recognition (CVPR)*, 2023.
- [56] C.-H. Lin, J. Gao, L. Tang, T. Takikawa, X. Zeng, X. Huang, K. Kreis, S. Fidler, M.-Y. Liu, and T.-Y. Lin. Magic3d: High-resolution text-to-3d content creation. In *IEEE Conference on Computer Vision and Pattern Recognition (CVPR)*, 2023.
- [57] M. Liu, C. Xu, H. Jin, L. Chen, M. Varma T, Z. Xu, and H. Su. One-2-3-45: Any single image to 3d mesh in 45 seconds without per-shape optimization. *Advances in Neural Information Processing Systems*, 36, 2024.
- [58] R. Liu, R. Wu, B. V. Hoorick, P. Tokmakov, S. Zakharov, and C. Vondrick. Zero-1-to-3: Zero-shot one image to 3d object. *ArXiv*, 2023.
- [59] Y. Liu, C. Lin, Z. Zeng, X. Long, L. Liu, T. Komura, and W. Wang. Syncdreamer: Generating multiview-consistent images from a single-view image. In *The Twelfth International Conference on Learning Representations*, 2024.



- [60] Y. Liu, S. Peng, L. Liu, Q. Wang, P. Wang, C. Theobalt, X. Zhou, and W. Wang. Neural rays for occlusion-aware image-based rendering. In *Proceedings of the IEEE/CVF Conference on Computer Vision and Pattern Recognition*, pages 7824–7833, 2022.
- [61] I. Loshchilov and F. Hutter. Decoupled weight decay regularization. In *International Conference on Learning Representations (ICLR)*, 2019.
- [62] S. Luo and W. Hu. Diffusion probabilistic models for 3d point cloud generation. *2021 IEEE/CVF Conference on Computer Vision and Pattern Recognition (CVPR)*, Jun 2021.
- [63] L. Melas-Kyriazi, C. Rupprecht, I. Laina, and A. Vedaldi. Realfusion: 360° reconstruction of any object from a single image. In *Arxiv*, 2023.
- [64] B. Mildenhall, P. P. Srinivasan, M. Tancik, J. T. Barron, R. Ramamoorthi, and R. Ng. Nerf: Representing scenes as neural radiance fields for view synthesis. In *ECCV*, 2020.
- [65] N. Müller, Y. Siddiqui, L. Porzi, S. R. Bulò, P. Kotschieder, and M. Nießner. Diffrrf: Rendering-guided 3d radiance field diffusion. In *Proceedings of the IEEE/CVF Conference on Computer Vision and Pattern Recognition*, pages 4328–4338, 2023.
- [66] T. Müller, A. Evans, C. Schied, and A. Keller. Instant neural graphics primitives with a multiresolution hash encoding. *ACM Trans. Graph.*, 41(4):102:1–102:15, July 2022.
- [67] T. Nguyen-Phuoc, C. Li, L. Theis, C. Richardt, and Y.-L. Yang. Hologan: Unsupervised learning of 3d representations from natural images. In *Proceedings of the IEEE/CVF International Conference on Computer Vision*, pages 7588–7597, 2019.
- [68] T. Nguyen-Phuoc, C. Richardt, L. Mai, Y.-L. Yang, and N. Mitra. Blockgan: Learning 3d object-aware scene representations from unlabelled images. In *Advances in Neural Information Processing Systems 33*, Nov 2020.
- [69] M. Niemeyer, J. T. Barron, B. Mildenhall, M. S. M. Sajjadi, A. Geiger, and N. Radwan. Regnerf: Regularizing neural radiance fields for view synthesis from sparse inputs. *2022 IEEE/CVF Conference on Computer Vision and Pattern Recognition (CVPR)*, Jun 2022.
- [70] J. J. Park, P. Florence, J. Straub, R. Newcombe, and S. Lovegrove. Deepsdf: Learning continuous signed distance functions for shape representation. In *Proceedings of the IEEE/CVF conference on computer vision and pattern recognition*, pages 165–174, 2019.
- [71] S. Peng, M. Niemeyer, L. Mescheder, M. Pollefeys, and A. Geiger. Convolutional occupancy networks. In *Computer Vision—ECCV 2020: 16th European Conference, Glasgow, UK, August 23–28, 2020, Proceedings, Part III 16*, pages 523–540. Springer, 2020.
- [72] B. Poole, A. Jain, J. T. Barron, and B. Mildenhall. Dreamfusion: Text-to-3d using 2d diffusion. *ArXiv*, 2022.
- [73] A. Radford and K. Narasimhan. Improving language understanding by generative pre-training. OpenAI, 2018.
- [74] J. Reizenstein, R. Shapovalov, P. Henzler, L. Sbordone, P. Labatut, and D. Novotny. Common objects in 3d: Large-scale learning and evaluation of real-life 3d category reconstruction. In *International Conference on Computer Vision*, 2021.
- [75] D. J. Rezende, S. Mohamed, and D. Wierstra. Stochastic backpropagation and approximate inference in deep generative models. In *International conference on machine learning*, pages 1278–1286. PMLR, 2014.
- [76] C. Rockwell, D. F. Fouhey, and J. Johnson. Pixelsynth: Generating a 3d-consistent experience from a single image. In *ICCV*, 2021.
- [77] B. Roessle, N. Müller, L. Porzi, S. R. Bulò, P. Kotschieder, and M. Nießner. Ganerf: Leveraging discriminators to optimize neural radiance fields. *ACM Trans. Graph.*, 42(6), nov 2023.
- [78] R. Rombach, A. Blattmann, D. Lorenz, P. Esser, and B. Ommer. High-resolution image synthesis with latent diffusion models. In *Proceedings of the IEEE/CVF Conference on Computer Vision and Pattern Recognition (CVPR)*, pages 10684–10695, June 2022.
- [79] R. Rombach, P. Esser, and B. Ommer. Geometry-free view synthesis: Transformers and no 3d priors. *ArXiv*, 2021.
- [80] O. Ronneberger, P. Fischer, and T. Brox. U-net: Convolutional networks for biomedical image segmentation. In *MICCAI*, 2015.
- [81] T. Salimans and J. Ho. Progressive distillation for fast sampling of diffusion models. In *International Conference on Learning Representations (ICLR)*, 2022.
- [82] J. L. Schönberger and J.-M. Frahm. Structure-from-motion revisited. In *Conference on Computer Vision and Pattern Recognition (CVPR)*, 2016.

- [83] C. Schuhmann, R. Beaumont, R. Vencu, C. Gordon, R. Wightman, M. Cherti, T. Coombes, A. Katta, C. Mullis, M. Wortsman, et al. Laion-5b: An open large-scale dataset for training next generation image-text models. *Advances in Neural Information Processing Systems*, 35:25278–25294, 2022.
- [84] K. Schwarz, Y. Liao, M. Niemeyer, and A. Geiger. GRAF: generative radiance fields for 3d-aware image synthesis. In H. Larochelle, M. Ranzato, R. Hadsell, M. Balcan, and H. Lin, editors, *Advances in Neural Information Processing Systems 33: Annual Conference on Neural Information Processing Systems 2020, NeurIPS 2020, December 6-12, 2020, virtual*, 2020.
- [85] K. Schwarz, S. Wook Kim, J. Gao, S. Fidler, A. Geiger, and K. Kreis. Wildfusion: Learning 3d-aware latent diffusion models in view space. In *International Conference on Learning Representations (ICLR)*, 2024.
- [86] S. M. Seitz, B. Curless, J. Diebel, D. Scharstein, and R. Szeliski. A comparison and evaluation of multi-view stereo reconstruction algorithms. In *2006 IEEE computer society conference on computer vision and pattern recognition (CVPR'06)*, volume 1, pages 519–528. IEEE, 2006.
- [87] S. M. Seitz and C. R. Dyer. Photorealistic scene reconstruction by voxel coloring. *International journal of computer vision*, 35:151–173, 1999.
- [88] Q. Shen, X. Yi, Z. Wu, P. Zhou, H. Zhang, S. Yan, and X. Wang. Gamba: Marry gaussian splatting with mamba for single view 3d reconstruction. *ArXiv*, 2024.
- [89] J. Shriram, A. Trevithick, L. Liu, and R. Ramamoorthi. RealmDreamer: Text-driven 3d scene generation with inpainting and depth diffusion. *ArXiv*, 2024.
- [90] J. R. Shue, E. R. Chan, R. Po, Z. Ankner, J. Wu, and G. Wetzstein. 3d neural field generation using triplane diffusion. *arXiv preprint arXiv:2211.16677*, 2022.
- [91] V. Sitzmann, J. Thies, F. Heide, M. Nießner, G. Wetzstein, and M. Zollhöfer. Deepvoxels: Learning persistent 3d feature embeddings. In *Proc. Computer Vision and Pattern Recognition (CVPR)*, IEEE, 2019.
- [92] I. Skorokhodov, S. Tulyakov, Y. Wang, and P. Wonka. Epigraf: Rethinking training of 3d gans. In S. Koyejo, S. Mohamed, A. Agarwal, D. Belgrave, K. Cho, and A. Oh, editors, *Advances in Neural Information Processing Systems*, volume 35, pages 24487–24501. Curran Associates, Inc., 2022.
- [93] N. Snavely, S. M. Seitz, and R. Szeliski. Photo tourism: exploring photo collections in 3d. In *ACM siggraph 2006 papers*, pages 835–846. 2006.
- [94] J. Sohl-Dickstein, E. A. Weiss, N. Maheswaranathan, and S. Ganguli. Deep unsupervised learning using nonequilibrium thermodynamics. *CoRR*, abs/1503.03585, 2015.
- [95] J. Song, C. Meng, and S. Ermon. Denoising diffusion implicit models. In *International Conference on Learning Representations*, 2021.
- [96] S. Szymanowicz, C. Rupprecht, and A. Vedaldi. Viewset diffusion: (0-)image-conditioned 3D generative models from 2D data. In *ICCV*, 2023.
- [97] S. Szymanowicz, C. Rupprecht, and A. Vedaldi. Splatter image: Ultra-fast single-view 3d reconstruction. *Conference on Computer Vision and Pattern Recognition (CVPR)*, 2024.
- [98] J. Tang, Z. Chen, X. Chen, T. Wang, G. Zeng, and Z. Liu. Lgm: Large multi-view gaussian model for high-resolution 3d content creation. *arXiv preprint arXiv:2402.05054*, 2024.
- [99] J. Tang, J. Ren, H. Zhou, Z. Liu, and G. Zeng. Dreamgaussian: Generative gaussian splatting for efficient 3d content creation. In *The Twelfth International Conference on Learning Representations*, 2024.
- [100] S. Tang, J. Chen, D. Wang, C. Tang, F. Zhang, Y. Fan, V. Chandra, Y. Furukawa, and R. Ranjan. Mvdifusion++: A dense high-resolution multi-view diffusion model for single or sparse-view 3d object reconstruction. *arXiv preprint arXiv:2402.12712*, 2024.
- [101] S. Tang, F. Zhang, J. Chen, P. Wang, and Y. Furukawa. MVDiffusion: Enabling holistic multi-view image generation with correspondence-aware diffusion. In *Thirty-seventh Conference on Neural Information Processing Systems*, 2023.
- [102] A. Tewari, T. Yin, G. Cazenavette, S. Rezchikov, J. B. Tenenbaum, F. Durand, W. T. Freeman, and V. Sitzmann. Diffusion with forward models: Solving stochastic inverse problems without direct supervision. In *Thirty-seventh Conference on Neural Information Processing Systems*, 2023.
- [103] H.-Y. Tseng, Q. Li, C. Kim, S. Alsisan, J.-B. Huang, and J. Kopf. Consistent view synthesis with pose-guided diffusion models. *ArXiv*, 2023.
- [104] A. Vahdat, F. Williams, Z. Gojcic, O. Litany, S. Fidler, K. Kreis, et al. Lion: Latent point diffusion models for 3d shape generation. *Advances in Neural Information Processing Systems*, 35:10021–10039, 2022.
- [105] A. van den Oord, S. Dieleman, H. Zen, K. Simonyan, O. Vinyals, A. Graves, N. Kalchbrenner, A. Senior, and K. Kavukcuoglu. Wavenet: A generative model for raw audio. In *Arxiv*, 2016.

- [106] A. Van Den Oord, N. Kalchbrenner, and K. Kavukcuoglu. Pixel recurrent neural networks. In *International conference on machine learning*, pages 1747–1756. PMLR, 2016.
- [107] A. Vaswani, N. Shazeer, N. Parmar, J. Uszkoreit, L. Jones, A. N. Gomez, L. u. Kaiser, and I. Polosukhin. Attention is all you need. In I. Guyon, U. V. Luxburg, S. Bengio, H. Wallach, R. Fergus, S. Vishwanathan, and R. Garnett, editors, *Advances in Neural Information Processing Systems*, volume 30. Curran Associates, Inc., 2017.
- [108] H. Wang, X. Du, J. Li, R. A. Yeh, and G. Shakhnarovich. Score jacobian chaining: Lifting pretrained 2d diffusion models for 3d generation. *ArXiv*, 2022.
- [109] H. Wang, X. Du, J. Li, R. A. Yeh, and G. Shakhnarovich. Score jacobian chaining: Lifting pretrained 2d diffusion models for 3d generation. In *Proceedings of the IEEE/CVF Conference on Computer Vision and Pattern Recognition*, pages 12619–12629, 2023.
- [110] Q. Wang, Z. Wang, K. Genova, P. Srinivasan, H. Zhou, J. T. Barron, R. Martin-Brualla, N. Snavely, and T. Funkhouser. Ibrnet: Learning multi-view image-based rendering. In *CVPR*, 2021.
- [111] T. Wang, B. Zhang, T. Zhang, S. Gu, J. Bao, T. Baltrusaitis, J. Shen, D. Chen, F. Wen, Q. Chen, and B. Guo. Rodin: A generative model for sculpting 3d digital avatars using diffusion. *ArXiv*, 2022.
- [112] Z. Wang, C. Lu, Y. Wang, F. Bao, C. Li, H. Su, and J. Zhu. Prolificdreamer: High-fidelity and diverse text-to-3d generation with variational score distillation. *Advances in Neural Information Processing Systems*, 36, 2024.
- [113] D. Watson, W. Chan, R. M. Brualla, J. Ho, A. Tagliasacchi, and M. Norouzi. Novel view synthesis with diffusion models. In *The Eleventh International Conference on Learning Representations*, 2023.
- [114] C. Wewer, K. Raj, E. Ilg, B. Schiele, and J. E. Lenssen. latentsplat: Autoencoding variational gaussians for fast generalizable 3d reconstruction. In *arXiv*, 2024.
- [115] O. Wiles, G. Gkioxari, R. Szeliski, and J. Johnson. Synsin: End-to-end view synthesis from a single image. In *Proceedings of the IEEE/CVF Conference on Computer Vision and Pattern Recognition*, pages 7467–7477, 2020.
- [116] C.-Y. Wu, J. Johnson, J. Malik, C. Feichtenhofer, and G. Gkioxari. Multiview compressive coding for 3d reconstruction. In *Proceedings of the IEEE/CVF Conference on Computer Vision and Pattern Recognition*, pages 9065–9075, 2023.
- [117] R. Wu, B. Mildenhall, P. Henzler, K. Park, R. Gao, D. Watson, P. P. Srinivasan, D. Verbin, J. T. Barron, B. Poole, and A. Holynski. Reconfusion: 3d reconstruction with diffusion priors. *ArXiv*, 2023.
- [118] T. Wu, J. Zhang, X. Fu, Y. Wang, L. P. Jiawei Ren, W. Wu, L. Yang, J. Wang, C. Qian, D. Lin, and Z. Liu. Omniobject3d: Large-vocabulary 3d object dataset for realistic perception, reconstruction and generation. In *IEEE/CVF Conference on Computer Vision and Pattern Recognition (CVPR)*, 2023.
- [119] J. Wynn and D. Turmukhambetov. DiffusioNeRF: Regularizing Neural Radiance Fields with Denoising Diffusion Models. In *CVPR*, 2023.
- [120] Y. Xie, T. Takikawa, S. Saito, O. Litany, S. Yan, N. Khan, F. Tombari, J. Tompkin, V. Sitzmann, and S. Sridhar. Neural fields in visual computing and beyond. *Computer Graphics Forum*, 2022.
- [121] Q. Xu, Z. Xu, J. Philip, S. Bi, Z. Shu, K. Sunkavalli, and U. Neumann. Point-nerf: Point-based neural radiance fields. In *Proceedings of the IEEE/CVF Conference on Computer Vision and Pattern Recognition*, pages 5438–5448, 2022.
- [122] Y. Xu, H. Tan, F. Luan, S. Bi, P. Wang, J. Li, Z. Shi, K. Sunkavalli, G. Wetzstein, Z. Xu, and K. Zhang. DMV3d: Denoising multi-view diffusion using 3d large reconstruction model. In *The Twelfth International Conference on Learning Representations*, 2024.
- [123] T. Yi, J. Fang, J. Wang, G. Wu, L. Xie, X. Zhang, W. Liu, Q. Tian, and X. Wang. Gaussiandreamer: Fast generation from text to 3d gaussians by bridging 2d and 3d diffusion models. In *CVPR*, 2024.
- [124] X. Yinghao, S. Zifan, Y. Wang, C. Hansheng, Y. Ceyuan, P. Sida, S. Yujun, and W. Gordon. Grm: Large gaussian reconstruction model for efficient 3d reconstruction and generation. *ArXiv*, 2024.
- [125] P. Yoo, J. Guo, Y. Matsuo, and S. S. Gu. Dreamsparse: Escaping from plato’s cave with 2d frozen diffusion model given sparse views. *CoRR*, 2023.
- [126] A. Yu, V. Ye, M. Tancik, and A. Kanazawa. pixelnerf: Neural radiance fields from one or few images. In *Proceedings of the IEEE/CVF Conference on Computer Vision and Pattern Recognition*, pages 4578–4587, 2021.
- [127] J. J. Yu, F. Forghani, K. G. Derpanis, and M. A. Brubaker. Long-term photometric consistent novel view synthesis with diffusion models. In *Proceedings of the International Conference on Computer Vision (ICCV)*, 2023.
- [128] X. Yu, M. Xu, Y. Zhang, H. Liu, C. Ye, Y. Wu, Z. Yan, T. Liang, G. Chen, S. Cui, and X. Han. Mvimnet: A large-scale dataset of multi-view images. In *CVPR*, 2023.

- [129] B. Zhang, Y. Cheng, J. Yang, C. Wang, F. Zhao, Y. Tang, D. Chen, and B. Guo. Gaussiancube: Structuring gaussian splatting using optimal transport for 3d generative modeling. *arXiv preprint arXiv:2403.19655*, 2024.
- [130] K. Zhang, S. Bi, H. Tan, Y. Xiangli, N. Zhao, K. Sunkavalli, and Z. Xu. Gs-irm: Large reconstruction model for 3d gaussian splatting. *ArXiv*, 2024.
- [131] R. Zhang, P. Isola, A. A. Efros, E. Shechtman, and O. Wang. The unreasonable effectiveness of deep features as a perceptual metric. In *Proceedings of the IEEE conference on computer vision and pattern recognition*, pages 586–595, 2018.
- [132] X. Zhao, F. Ma, D. Güera, Z. Ren, A. G. Schwing, and A. Colburn. Generative multiplane images: Making a 2d gan 3d-aware. In *Proc. ECCV*, 2022.
- [133] S. Zheng, B. Zhou, R. Shao, B. Liu, S. Zhang, L. Nie, and Y. Liu. Gps-gaussian: Generalizable pixel-wise 3d gaussian splatting for real-time human novel view synthesis. In *Proceedings of the IEEE/CVF Conference on Computer Vision and Pattern Recognition (CVPR)*, 2024.
- [134] L. Zhou, Y. Du, and J. Wu. 3d shape generation and completion through point-voxel diffusion. In *Proceedings of the IEEE/CVF International Conference on Computer Vision*, pages 5826–5835, 2021.
- [135] T. Zhou, R. Tucker, J. Flynn, G. Fyffe, and N. Snavely. Stereo magnification: Learning view synthesis using multiplane images. *ACM Trans. Graph. (Proc. SIGGRAPH)*, 37, 2018.
- [136] Z. Zhou and S. Tulsiani. Sparsefusion: Distilling view-conditioned diffusion for 3d reconstruction. In *CVPR*, 2023.
- [137] J. Zhu and P. Zhuang. Hifa: High-fidelity text-to-3d with advanced diffusion guidance. *arXiv preprint arXiv:2305.18766*, 2023.
- [138] Z.-X. Zou, W. Cheng, Y.-P. Cao, S.-S. Huang, Y. Shan, and S.-H. Zhang. Sparse3d: Distilling multiview-consistent diffusion for object reconstruction from sparse views. *arXiv preprint arXiv:2308.14078*, 2023.
- [139] Z.-X. Zou, Z. Yu, Y.-C. Guo, Y. Li, D. Liang, Y.-P. Cao, and S.-H. Zhang. Triplane meets gaussian splatting: Fast and generalizable single-view 3d reconstruction with transformers. *ArXiv*, 2023.

## A Implementation Details

**Optimisation.** We train using AdamW [61] with a cosine learning rate schedule having maximum value  $6 \times 10^{-5}$  and 500 steps for warm-up. For regularisation, we use weight decay with strength  $4 \times 10^{-2}$ , and dropout with probability 0.28 after each U-Net block. Total batch size is 24 for the autoencoder and 64 for the denoiser. For the denoiser, we use a linear noise schedule over 1000 steps, with  $v$ -prediction as the objective [81]. These hyperparameters were chosen using automated random sweeps, choosing the best-performing based on validation-set PSNR for single-image reconstruction. During autoencoder training the KL weight  $\beta$  is set to 0.1, and we give the L2 and LPIPS losses equal weight. We train with class conditioning (or unconditional for RealEstate10K) for 40% of batches, image conditioning (for single-image reconstruction) for 40% of batches, and no conditioning (to enable CFG) for the remaining 20%.

**View selection.** During autoencoder training, we select groups of six frames from the videos as input to our model; these are drawn with stratified sampling so they are roughly evenly spaced through the entire original video clip, minimising visual ambiguity. The autoencoder is trained to reconstruct six immediately-adjacent frames (each randomly chosen as preceding or following an input frame); this discourages pathological solutions with trivial 3D geometry that can arise when reconstructing the exact input frames. During denoiser training, we again sample sets of input views following the same strategy. No disjoint target views are required for this stage since pathological solutions do not arise in the latent space. When training with image conditioning, we randomly select one view to use as the conditioning image, and pass this separately through the encoder  $E$ . For testing single-image reconstruction, we sample 12 views per scene. The middle view was used as the input for MVImgNet and the first view for RealEstate10K; reconstruction metrics are calculated on the remaining 11 views. For testing sparse-view reconstruction, we sample 12 views per scene, using alternate views for input and evaluation. For testing unconditional/class-conditional generation, we use randomly chosen sets of six camera poses from the validation set.

**Splatter Image.** We utilized the publicly available implementation from the original authors, training it on the same splits of MVImgNet and RealEstate10K as our model. During training, we processed mini-batches of scenes, each consisting of six posed views selected as for our model. One view was randomly chosen as the input, while the remaining views served as ground truth to optimize the model by comparing the generated renderings with the true images. For both datasets, we enable prediction of 3D splat offsets. For testing, the middle view was used as the input for MVImgNet, and the first view for RealEstate10K.

## B Additional Results

### B.1 Denoised vs heldout views

Here we measure how the quality of generated scenes varies between ‘denoised’ and ‘held-out’ views. The denoised views are those on which we support both the splats and the latent representation  $z_v$ ; the held-out views are evenly spaced between these (i.e. as far from them as possible). It is natural to consider whether our image-centric approach encourages higher-quality images from the denoised viewpoints. However, we find (see Table 3) that there is only minimal difference—FID is slightly better on diffused views for both datasets, while held-out views actually show fractionally better reconstruction metrics.

### B.2 Additional Qualitative results

Figures 6–8 give additional qualitative results, following the same protocol as the corresponding figures in the paper. Please refer to the respective captions for details.

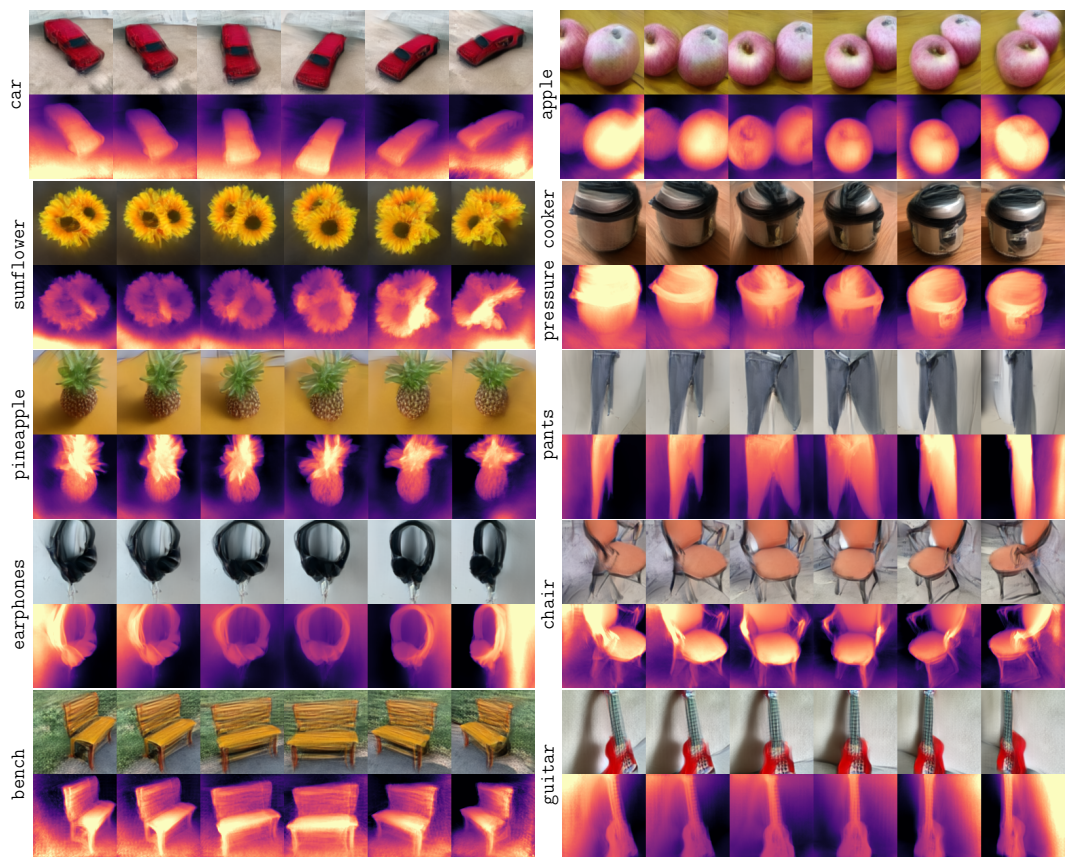
## C Compute Requirements

Our final models each trained for 24 GPU-days on a local cluster, on nodes with  $4 \times$  NVIDIA A5000 GPUs (24GB VRAM) and single 16-core CPU with 128GB RAM; we used either two or four GPUs per run. SplatterImage trained for approximately 4 GPU-days on the same hardware, using a single

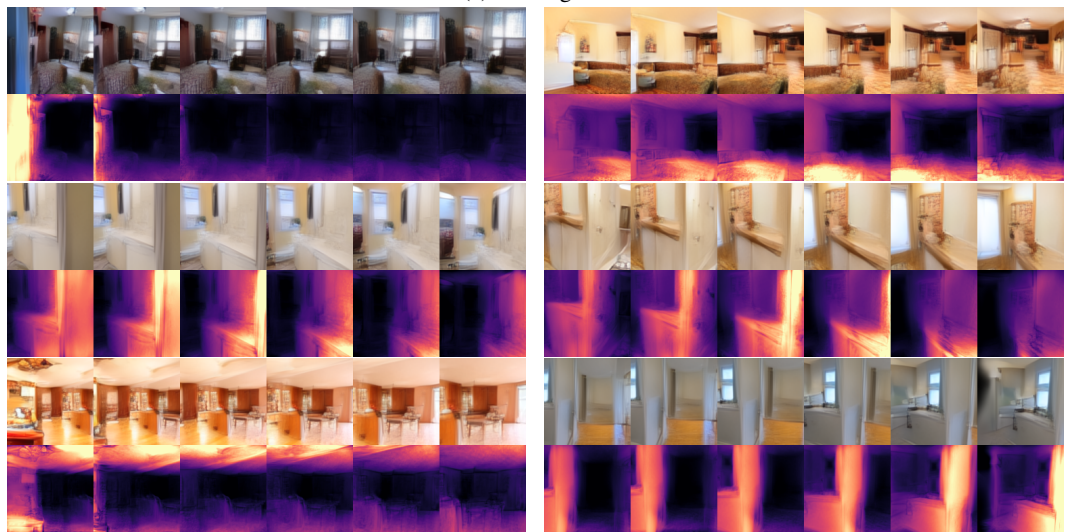
Table 3: Quality of denoised views, compared with and held-out views placed between them. Comparable values indicate that although denoising occurs (and splats are supported on) a subset of views, the 3D shape also re-renders accurately to other views

|               | <b>diffused</b> |        |         | <b>held-out</b> |        |         |
|---------------|-----------------|--------|---------|-----------------|--------|---------|
|               | FID ↓           | PSNR ↑ | LPIPS ↓ | FID ↓           | PSNR ↑ | LPIPS ↓ |
| MVImgNet      | 22.8            | 20.3   | 0.332   | 23.6            | 20.9   | 0.318   |
| RealEstate10K | 29.3            | 16.4   | 0.457   | 29.9            | 16.5   | 0.453   |

GPU per run. The total compute for the project (including preliminary runs and hyperparameter sweeps) is estimated at 2500 GPU-days.



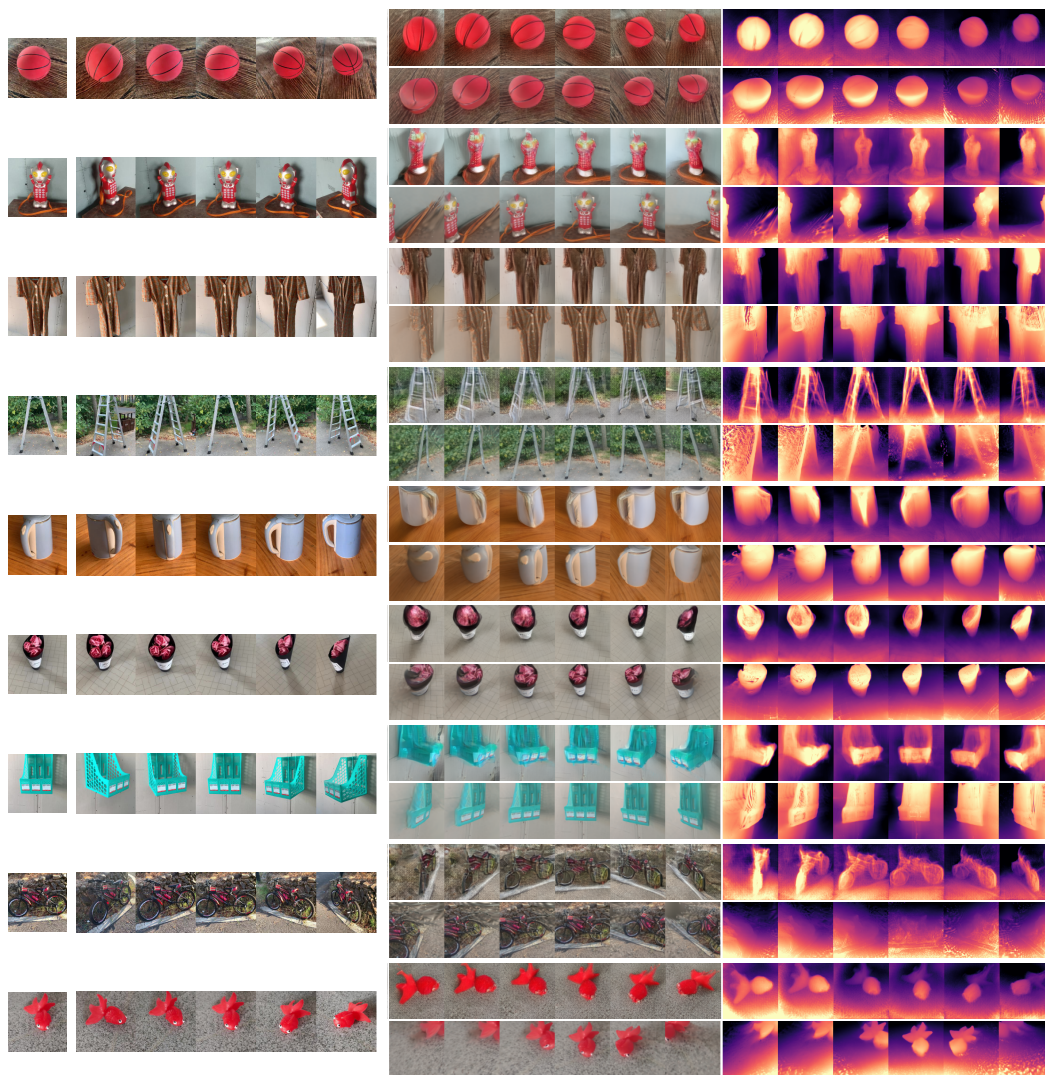
(a) MVImgNet



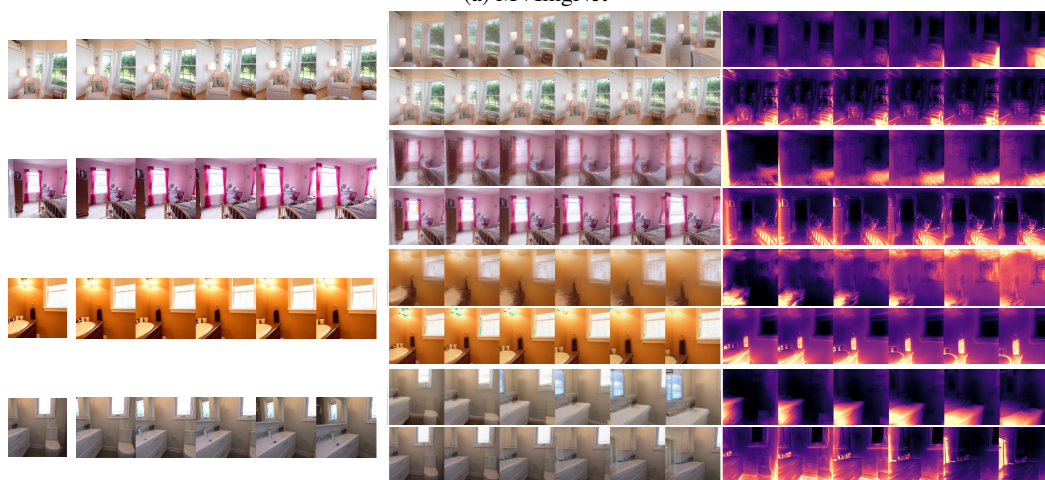
(b) RealEstate10K

Figure 6: Additional qualitative examples of class-conditional (MVImgNet) and unconditional generations (RealEstate10K) from our method. For each example, the top row shows six rendered views of the sampled 3D scene, while the bottom row shows the corresponding depths.





(a) MVImgNet



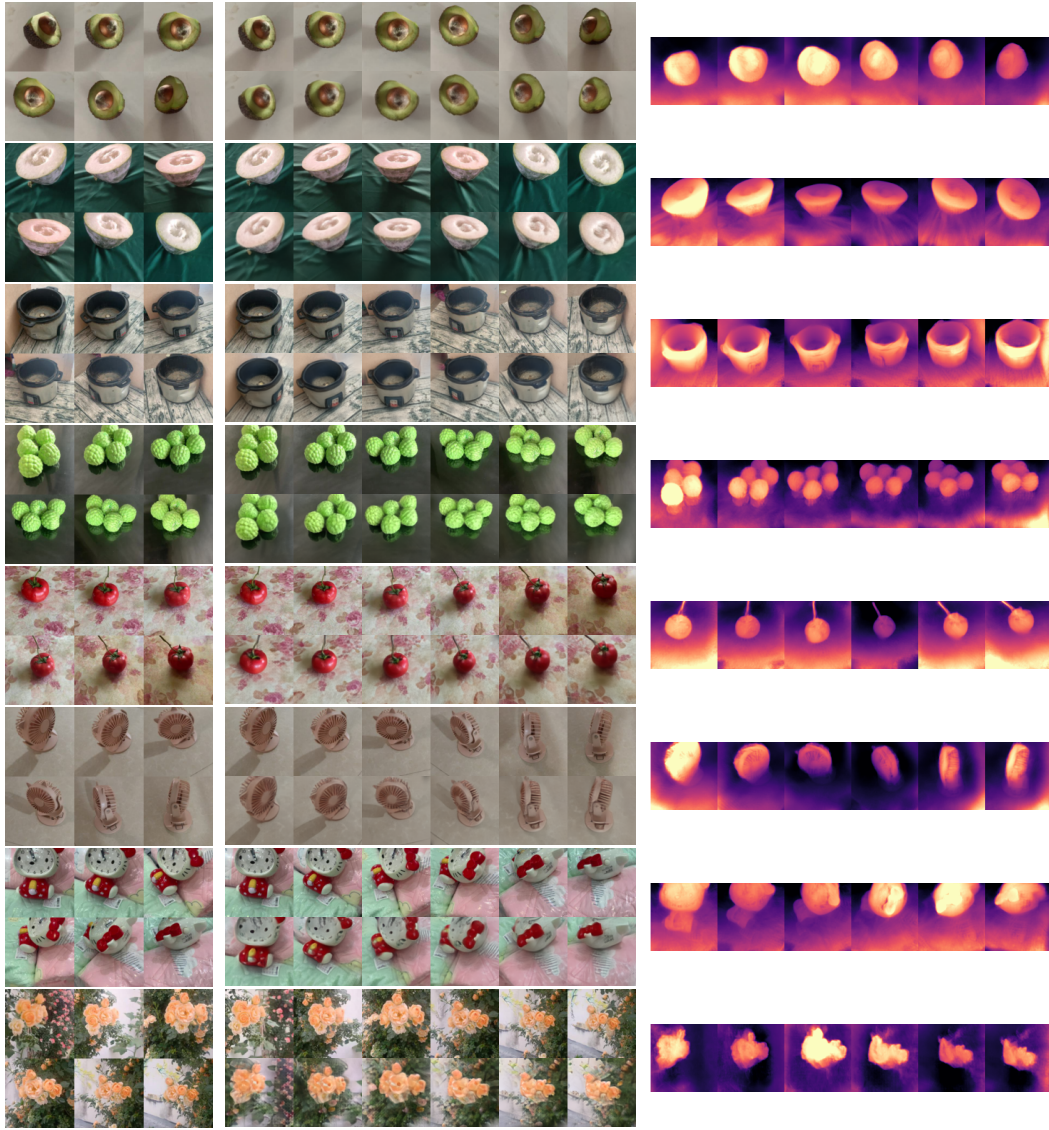
(b) RealEstate10k

Figure 7: Additional qualitative comparison of 3D reconstruction from a single image between our model (upper row of each pair) and SplatterImage (lower row of each pair) on MVImgNet (a) and RealEstate10k (b). The first column shows the input (conditioning) image, the second displays the ground truth images, and the third and fourth columns display the predicted frames and depths, respectively.

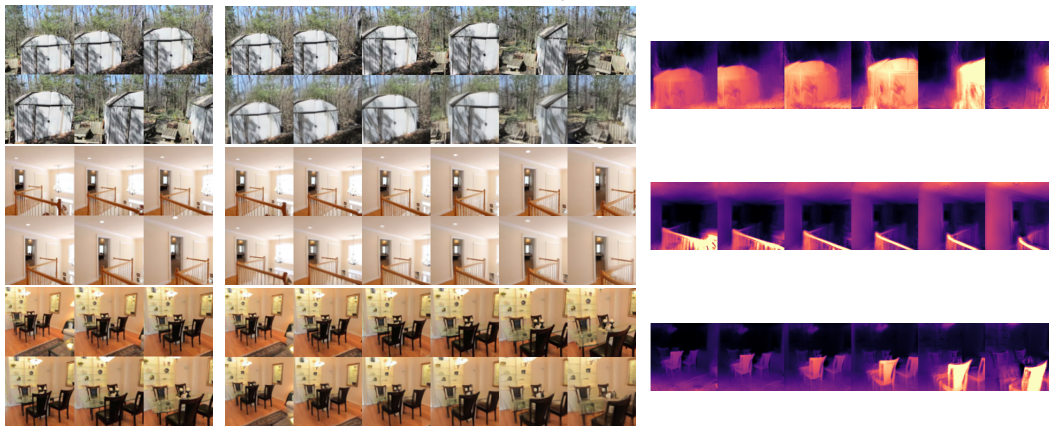




Figure 8: Additional qualitative results for 3D reconstruction from a single image showing diversity of sampled 3D assets. Given a single view as input (first column), our model samples 3D scenes from the posterior distribution (center columns). In contrast to a deterministic baseline, which outputs averaged blurry solution (last column), our model samples diverse plausible back-views



(a) MVIImageNet



(b) RealEstate10k

Figure 9: Additional qualitative results for 3D reconstruction from six images from our model on MVIImageNet (a) and RealEstate10k (b) datasets. First column shows input (conditioning) images, second column shows the ground truth images (above) and images rendered from the sampled 3D scene (below), while the third column shows its corresponds depths.